JPE 19-5-15

https://doi.org/10.6113/JPE.2019.19.5.1216
ISSN(Print): 1598-2092 / ISSN(Online): 2093-4718

Sensorless Control of Double-Sided Linear Switched Reluctance Machines with Eccentricities

Qianlong Wang†, Zhengfei Wu*, and Wei Jiang*

†,*Department of Electrical Engineering, Yangzhou University, Yangzhou, China

Abstract

The Double-sided Linear Switched Reluctance Machine (DLSRM) suffers from complex eccentricities in practical operations. A novel sensorless control method for a DLSRM with eccentricities is developed in this paper. The influences of eccentricities on the machine inductance characteristics and the estimated positions in sensorless control systems are discussed. A new position index, which is independent of eccentricities, is proposed according to an analysis of a DLSRM equivalent magnetic circuit. On the basis of this position index, the starting and low-velocity operation of eccentric DLSRMs are achieved. Experimental results obtained in the laboratory validate the proposed method.

Key words: Double-sided linear switched reluctance machine, Eccentricity, Position estimation, Sensorless control

I. INTRODUCTION

Double-sided linear switched reluctance machines (DLSRMs) have been attracting the attention of a lot of researchers in recent years owing to their merits of non-normal forces and high thrust-to-mass ratio [1]-[4]. Like rotary SRMs, the position sensors in DLSRMs decrease the reliability and increase the cost of the drive system. Research on the sensorless control of SRMs has been developed for almost three decades. Many sensorless control methods have been proposed such as the current-waveform-based method [5], chopping-currents-slope-based method [6], inductance-model-based method [7]-[9], flux-linkage-based method [10], etc.

For the starting and low-speed operation of SRMs, the voltage pulse injection method (VPIM) is the most-frequently used scheme [5], [8], [11]-[12]. In the VPIM, high-frequent voltage pulses are injected into idle phases, and position information can be obtained from the peak values of the response currents [11], the currents rising/falling time [5], the currents slope differences [8], etc. The detection principle of the VPIM is a one-to-one correspondence between machine characteristics such as inductances and the fluxes, and the rotor/mover relative positions. In [11], the mover positions of a single-sided LSRM are estimated according to the integrate values of the response currents in the VPIM.

However, in a previous work [13], it was shown that the problem of the eccentricities is inevitable in the practical operation of DLSRMs due to the three factors.

i) Manufacturing errors - manufacturing and laminating errors of the silicon steel sheets and the rails or guides.

ii) Wear and tear of the guides or rails - after a long period of operation, there is wear and tear on the guides or rails, and the air gaps become unbalanced.

iii) Assembling error - assembling errors of the guides or rails and the movers, especially for the long stroke situation. For the long stroke situation, the movers of the linear machine are always sectional. Then assembling errors and unbalanced air gaps become inevitable.

The machine characteristics of DLSRM change with eccentricities, which increases the errors of the estimated positions and makes the sensorless control system unstable. Little attention has been paid to the sensorless control of DLSRMs with eccentricities. A new method of inductance estimation for LSRMs without eccentricity was proposed in [14] to improve the conventional sensorless control precision. [13] and [15] focused on unbalanced force reduction of eccentric DLSRMs. A novel position estimation method for DLSRMs without eccentricities was given in [12] according to the eddy-current effect.

A sensorless control method of DLSRMs with different eccentricities is developed in this study. The main contribution

Manuscript received Aug. 14, 2018; accepted Apr. 18, 2019
Recommended for publication by Associate Editor Young-Doo Yoon.
†Corresponding Author: qianlong881230@126.com
Tel: +86-138-1314-8411, Fax: +86-0514-87971315, Yangzhou Univ.
*Department of Electrical Engineering, Yangzhou University, China

of this paper is to find a new position index, which is independent of eccentricities. On the basis of the position index, the starting and low-velocity operations of eccentric DLSRMs are achieved.

The research in this paper focuses on the sensorless control of eccentric DLSRMs. This paper is organized as follows. The influences of eccentricities on a DLSRM sensorless control system are analyzed in Section II. A novel position index for DLSRMs with different eccentricities is proposed in Section III. A starting and low-velocity sensorless control method is carried out in Section IV. All of the methods are verified by prototype experimental results in Section V. Finally, some conclusions are summarized in Section VI.

II. Influences of Eccentricities on Sensorless Control Systems

Fig. 1 shows the structure of the test DLSRM, the dimensions of which were presented in [13]. The eccentricity ε is defined as:

$$\varepsilon=\frac{g_u-g_d}{g}\times 100\% \tag{1}$$

where g is the designed thickness of the machine air-gap (in this research, g=1.5 mm), and g_u and g_d represent the thicknesses of the air-gaps on both sides of the mover (i.e. the upside air-gap thickness and the downside air-gap thickness). As shown in Fig. 1, when the mover has an upward displacement, the length of the upside air gap g_u is smaller than that of the downside air gap g_d. Then the eccentricity ε is negative. Similarly, when the mover has a downside displacement, the eccentricity ε is positive. The turns of the coil on each pole is 160, and one phase winding contains four series coils. Take phase A as an example, the phase winding of phase A consists of the coils A_1, A_2, A_3 and A_4. The current directions in each coil are described by the symbols of ⊗ and ⊙ in Fig. 1.

The phase unsaturated inductances at the different mover positions of an eccentric DLSRM are obtained by three-dimensional finite element analysis, as depicted in Fig. 2. This figure shows that the phase inductances increase with the eccentricities, especially at the overlap positions of the stator and mover poles. For a healthy DLSRM (without eccentricity, ε=0%) the maximum phase inductance is about 237 mH, while for a DLSRM with 50% eccentricity, the value increases to 285 mH. The minimum phase inductance remained approximately constant. In the sensorless control system of a DLSRM, inductance profiles are usually utilized to estimate the mover positions. When the air-gap thicknesses g_u and g_d are unequal, i.e. the machine becomes eccentric, differences in the phase inductances between the healthy DLSRM and the eccentric DLSRM lead to evaluation errors of the mover positions. In the healthy DLSRM, a phase inductance value of 237 mH corresponds to the fully aligned position (i.e. mover position is 30 mm for the test DLSRM, as

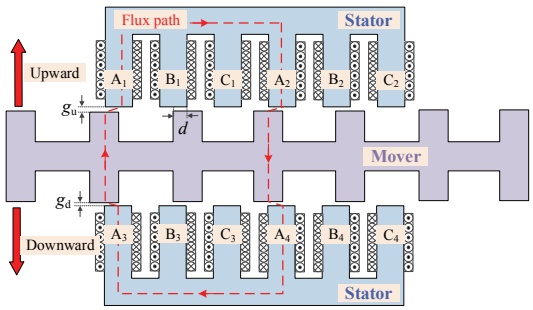

Fig. 1. Structure of the test DLSRM.

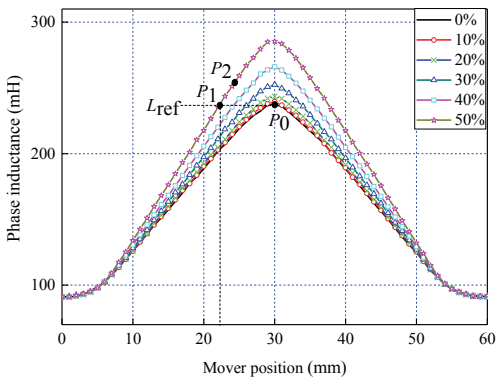

Fig. 2. Inductance profiles of a DLSRM with different eccentricities.

indicated by point P_0 in Fig. 2). When the machine has an eccentricity of 50% (g_u=0.75 mm, g_d=2.25 mm), a phase inductance of 237 mH corresponds to a mover position of 22 mm. That is, an air-gap deviation of 0.75 mm results in an estimated position error of 8 mm. Moreover, if the measured phase inductance is higher than the maximum inductance of the healthy machine, such as point P_2 in Fig. 2, the higher inductance values are not in the mapping range, and the controller outputs an inaccurate evaluated mover position. Therefore, it is necessary to take eccentricity into consideration in the sensorless control of a DLSRM.

III. New Position Index

The proposed scheme is feasible for the sensorless control system of an eccentric DLSRM building a three-dimensional lookup-table of the phase inductance regarding the mover positions and eccentricities. The main disadvantage of this method is a large amount of necessary data in the lookup-table, which needs to be obtained by finite element analysis or prototype testing. There are heavy computations, tests and memory burdens in previously prepared lookup-tables. A new position index, which is independent of machine eccentricities, is proposed in this paper to simplify the sensorless control process of eccentric DLSRMs.

A. Magnetic Circuit Analysis

The simplified magnetic circuit of a DLSRM is presented

in Fig. 3, where the flux leakage and fringing flux are neglected. R_s, R_m, R_u and R_d represent the reluctances of the stator yoke, mover yoke, upside air-gap and downside air-gap, respectively. F_1-F_4 represent magnetomotive forces of coils B_1-B_4, respectively. If the current in coils B_1 and B_2 is i_u, and the current in coils B_3 and B_4 is i_d, then $F_1=F_2=Ni_u$ and $F_3=F_4=Ni_d$, where N is the number of coils B_1-B_4. The reluctance of the ferromagnetic material is small enough to be ignored when compared with the air-gaps. Therefore, the whole magnetic circuit can be simply solved by the two independent magnetic circuits, Circuit-1 and Circuit-2, shown in Fig. 3.

The total reluctance of R^u_{tot} and R^d_{tot} in Circuit-1 and Circuit-2 can be simply expressed as:

$$\begin{cases} R^{u}_{tot} \approx 2R_u + R_s + R_m \approx 2\dfrac{g(1+\varepsilon)}{\mu_0(d*l)} + R_s + R_m \\ R^{d}_{tot} \approx 2R_d + R_s + R_m \approx 2\dfrac{g(1-\varepsilon)}{\mu_0(d*l)} + R_s + R_m \end{cases} \tag{2}$$

where d is the overlap distance between the stator and the mover pole (shown in Fig. 1), l is the stack length of the DLSRM, and μ_0 is the vacuum permeability.

Since the reluctances of R_s and R_m are much smaller than R_u and R_d, the total reluctance can be simplified as:

$$\begin{cases} R^{u}_{tot} \approx 2\dfrac{g(1+\varepsilon)}{\mu_0(d*l)} \\ R^{d}_{tot} \approx 2\dfrac{g(1-\varepsilon)}{\mu_0(d*l)} \end{cases} \tag{3}$$

The coils B_1 and B_2 are connected in series as the winding in Circuit-1. Similarly, the winding in Circuit-2 is composed of the coils B_3 and B_4. The unsaturated self-inductance of the windings in Circuit-1 and Circuit-2 can be simply derived as:

$$\begin{cases} L_u \approx \dfrac{(2N)^2}{2\dfrac{g(1+\varepsilon)}{\mu_0(d*l)}} = \dfrac{2N^2\mu_0(d*l)}{g(1+\varepsilon)} \\ L_d \approx \dfrac{(2N)^2}{2\dfrac{g(1-\varepsilon)}{\mu_0(d*l)}} = \dfrac{2N^2\mu_0(d*l)}{g(1-\varepsilon)} \end{cases} \tag{4}$$

From (4), it can be observed that the inductances on both sides change with the eccentricities. A relationship exists between L_u and L_d as:

$$R_L = \frac{1}{L_u} + \frac{1}{L_d} \approx \frac{g}{N^2\mu_0(d*l)} \tag{5}$$

It can be found that air-gap shifting alters the phase inductances and the inductances of the windings in Circuit-1 and Circuit-2. Nevertheless, the reciprocal sum of the two inductances L_u and L_d (defined as R_L in this paper) is independent of eccentricities and has an inverse correlation with the overlap distance d. Therefore, a two-dimensional lookup-table or a fitting polynomial can be formed by building a mapping between R_L and the overlap d. In addition, the computation, test and memory burden are all effectively decreased in the sensorless control system of an eccentric DLSRM.

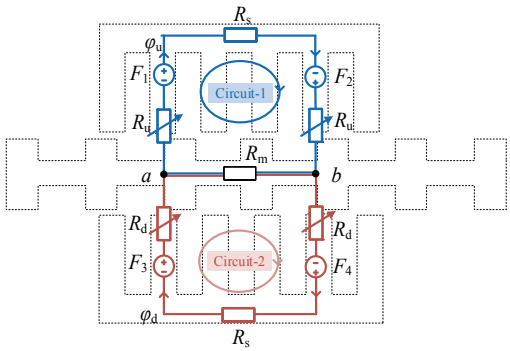

Fig. 3. Equivalent magnetic circuit of a DLSRM.

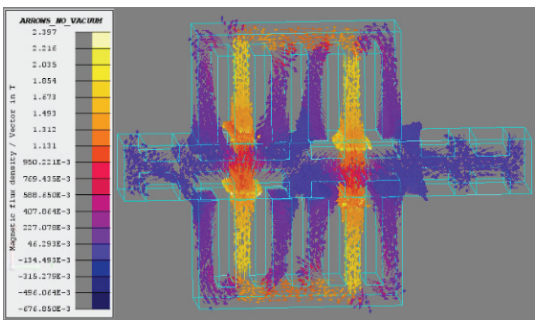

Fig. 4. Finite element model of a DLSRM.

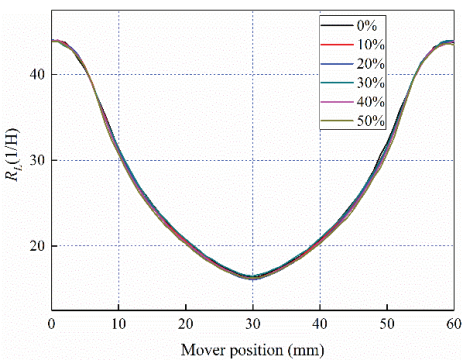

Fig. 5. Calculated RL values against positions of a DLSRM with different eccentricities.

B. Finite Element Analysis

To verify the correctness of (5), the DLSRM inductances are calculated by the three-dimensional finite element method and measured by a machine prototype. A finite element analysis model of a DLSRM is shown in Fig. 4. Fig. 5 and Fig. 6 give the calculated and measured R_L-eccentricities-position curves, respectively. The finite element calculation results shown in Fig. 5 illustrate that when the DLSRM eccentricities vary from 0% to 50%, the R_L values are almost unchanged. In addition, the R_L values have a monotonous relationship with the motor positions. The results of the prototype test shown in Fig. 6 also verify the analyses. The errors of the calculated and tested R_L curves, which are mainly

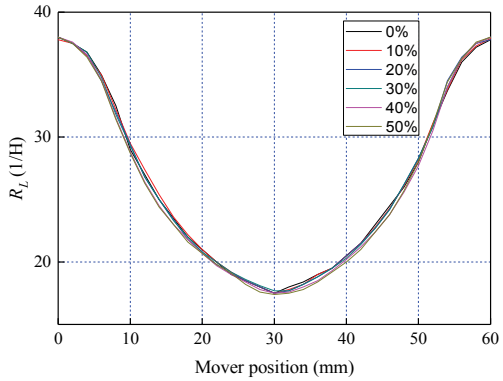

Fig. 6. Measured RL values against positions of a DLSRM with different eccentricities.

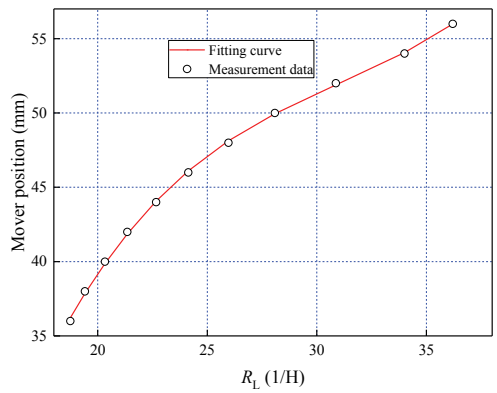

Fig. 7. Polynomial fitting results of the positions against R_L.

distributed at positions with lower inductances, are mainly caused by neglect of winding resistance voltage drops, prototype manufacturing errors, and *B-H* curve errors of the core material in the finite element model.

Based on the proposed position index R_L, the position mapping zone is determined according to the following factors. Pulses should be injected into the inductance drop zone of each phase. Overlap between the excitation currents and the injected pulse currents should be avoided. The position index curve in the mapping zone should have a large slope. For the test DLSRM in this paper, a mover position interval from 36 mm to 56 mm is selected to achieve the position estimation according to the R_L curves in Fig. 6 (the thick lines). The polynomial fitting method is carried out by least squares fitting to describe the characteristic relationship of R_L and the mover positions, as shown in Fig. 7. The polynomial fitting function is given as:

$$P_m = 0.0042R_L^3 - 0.3896R_L^2 + 12.73R_L - 95.1256 \quad (6)$$

where P_m is the mover position.

IV. Sensorless Control Method

Fig. 8 gives a DLSRM three-phase R_L curve, where the horizontal coordinate is the relative mover position of phase

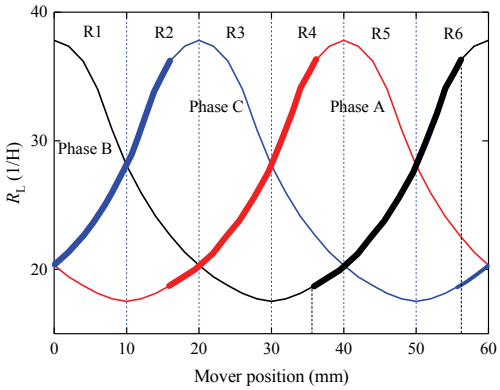

Fig. 8. Values of R_L for the three phases of a DLSRM.

TABLE I
Starting Order of a DLSRM

Regions	Order of R_A, R_B, R_C	Excited phases	Injected phases
R1	$R_B > R_C \geq R_A$	A, B	C
R2	$R_C \geq R_B > R_A$	B	C
R3	$R_C > R_A \geq R_B$	B, C	A
R4	$R_A \geq R_C > R_B$	C	A
R5	$R_A > R_B \geq R_C$	A, C	B
R6	$R_B \geq R_A > R_C$	A	B

B. The R_L curves of phase A, phase B and phase C differ by 20 mm with respect to each other. The whole mover position cycle can be divided into 6 regions by the three R_L curves of the three phases, which are R1 (0 mm~10 mm), R2 (10 mm~20 mm), R3 (20 mm~30 mm), R4 (30 mm~40 mm), R5 (40 mm~50 mm) and R6 (50 mm~60 mm). The R_L values of phase A, phase B and phase C are labeled as R_A, R_B and R_C, respectively.

To start the DLSRM, voltage pulses are injected in all three phases and the R_L values are detected. By comparing the R_L values of the three phases, the excited phases and the pulse injected phases are determined by the rules listed in Table I. After starting the DLSRM, the continuous mover position information can be obtained through (6), where the R_L values are measured based on the current pulses of the injected phases. The inductance estimation of the coils (L_u and L_d) in the test DLSRM have been presented in detail in [14] as follows:

$$L_{u/d} = 2\left(U_s - 2U_{\Delta T}\right)\frac{\Delta t_1}{\Delta I} - \left(U_s + 2U_{\Delta D}\right)\frac{\Delta t_2}{\Delta I} \quad (7)$$

where U_s is the DC power supply voltage, $U_{\Delta T}$ and $U_{\Delta D}$ are the voltage drop of the switch and the diode, respectively, Δt_1 is the energizing interval, Δt_2 is the de-energizing interval, and ΔI is the peak value of the measured response current.

The power converter proposed in [15] was utilized in this study to measure the inductances of L_u and L_d at the same time, as shown in Fig. 9. Take phase A as an example. If phase

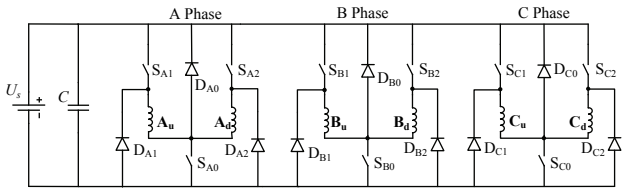

Fig. 9. Structure of a power converter.

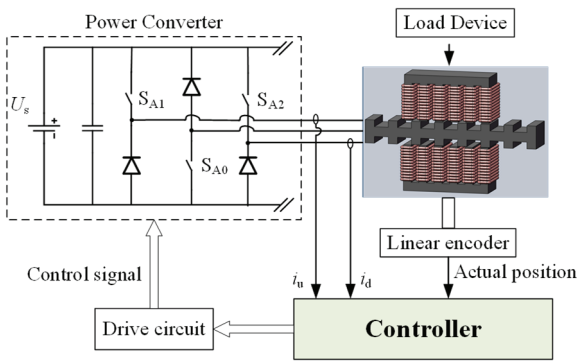

Fig. 10. Diagram of the control system for the sensorless control of an eccentric DLSRM.

A is the injected phase, the switches S_{A1}, S_{A2} and S_{A0} should be turn on/off at the same time at a high frequency. The switches S_{A0} and S_{A1} are controlled to turn on/off coil A_u in phase A. Similarly, S_{A0} and S_{A2} are related to coil A_d. The power converter can also be explored in terms of the unbalanced forces reduction of a DLSRM, as described in [15]. A control block diagram of the whole system is shown in Fig. 10.

Fig. 11 illustrates a flow chart of the sensorless starting and low-velocity operation control of an eccentric DLSRM. Take phase A as an example. The main procedures of the sensorless control algorithm are as follows.

1) For starting the DLSRM, high frequent voltage pulses (5 kHZ in this paper) are injected into three phases at the same time. Then the coils inductances in Circuit-1 and Circuit-2 (i.e. L_u and L_d) are estimated via (7).

2) Calculate the R_L value via (5). Then decide the excited phases and the injected phases via Table I.

3) Hysteresis loop control is used in the excited phases, as described in [15], and high frequent voltage pulses are injected into the injected phases.

4) Calculate the R_L value of the injected phases via (5). Then calculate the mover position P_m via (6).

5) Judge whether the excited phase is in the turn-on interval ($x_{off} \geq P_m \geq x_{on}$). If the mover position of the excited phase is in the turn-on interval, turn on the corresponding excited phases. Otherwise, turn off the phases.

6) Judge whether the injected phase is in the mapping zone (36 mm-56 mm in this paper). If the value of P_m is out of the mapping zone (i.e. P_m>56 mm), change the injected phase to another phase.

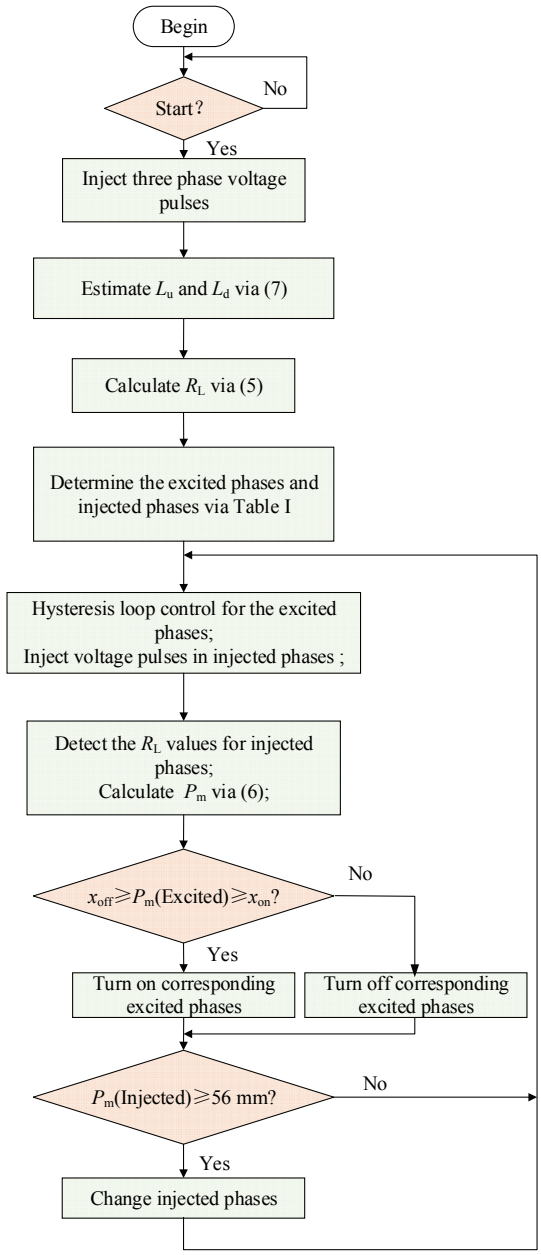

Fig. 11. Flow chart of the starting and low-velocity operation for an eccentric DLSRM.

V. Verification and Result Analysis

To verify the proposed method, a prototype experiment platform was designed. Photographs of the platform are shown in Fig. 12. In the platform, a linear encoder is used to obtain the actual mover positions, and a magnetic powder brake is chosen to load the DLSRM. A TI TMS320F28335 DSP acts as the controller. The air-gap thicknesses can be regulated from 0 to 5 mm by adjusting position nuts.

First, the air gap is adjusted to make the DLSRM eccentricity 0% (g_u=g_d=1.5 mm), the dc power supply voltage 24 V is supplied, the turn-on position is 0 mm, and the turn-off position is 22 mm. Fig. 13(a) shows result of the measured

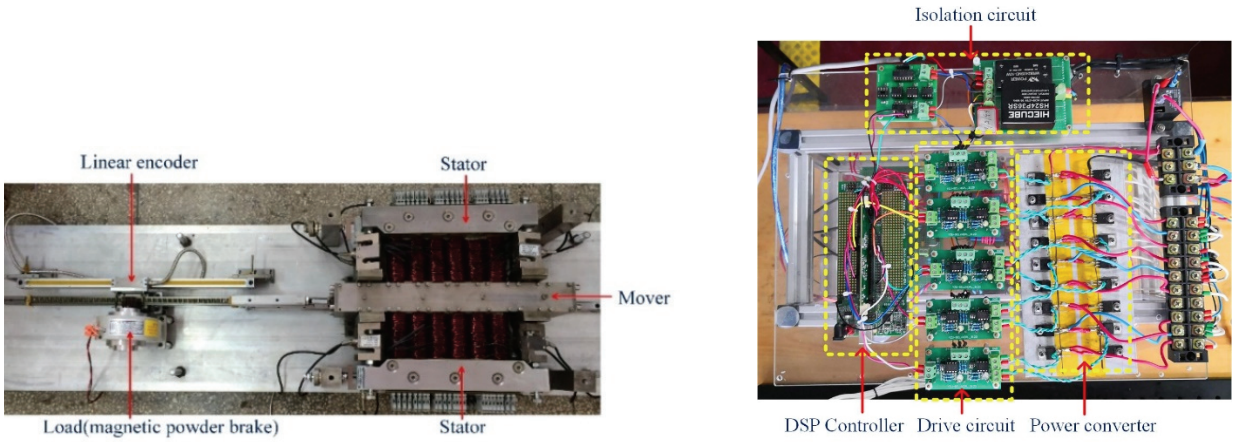

(a) (b)

Fig. 12. Photographs. (a) DLSRM prototype. (b) Control system hardware platform.

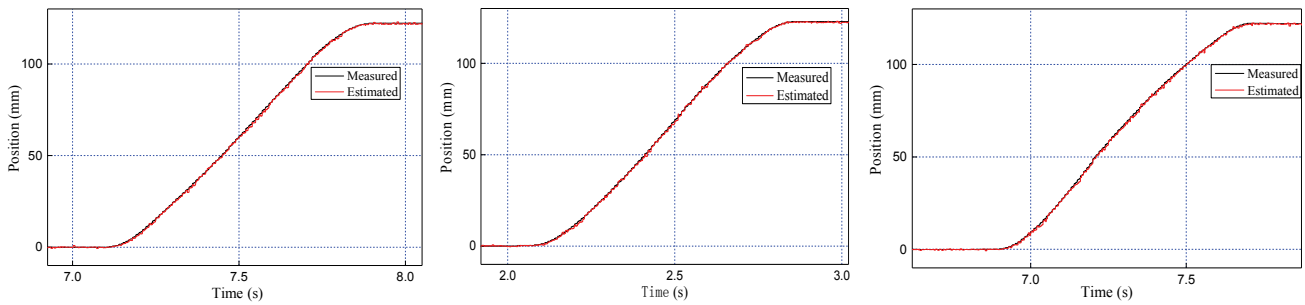

(a) (b) (c)

Fig. 13. Position estimation results of a DLSRM with different eccentricities (velocity: 0.15 m/s). (a) ε=0%. (b) ε=20%. (c) ε=40%.

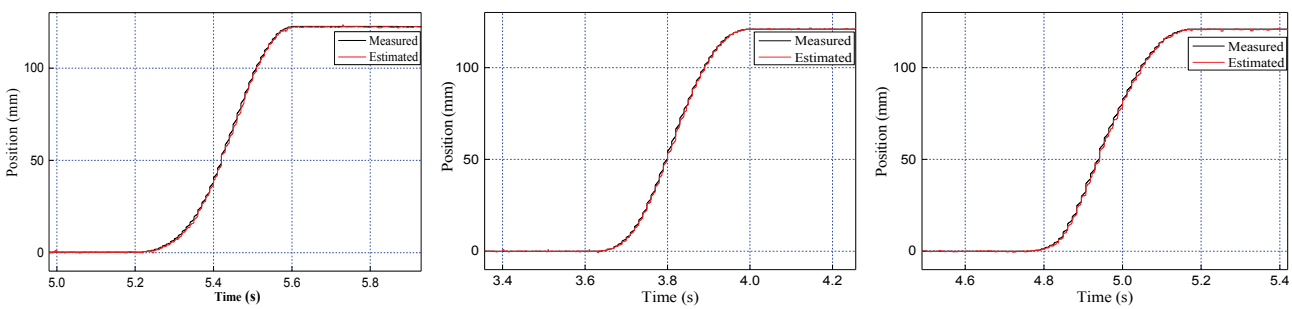

(a) (b) (c)

Fig. 14. Position estimation results of a DLSRM with different eccentricities (velocity: 0.30 m/s). (a) ε=0%. (b) ε=20%. (c) ε=40%.

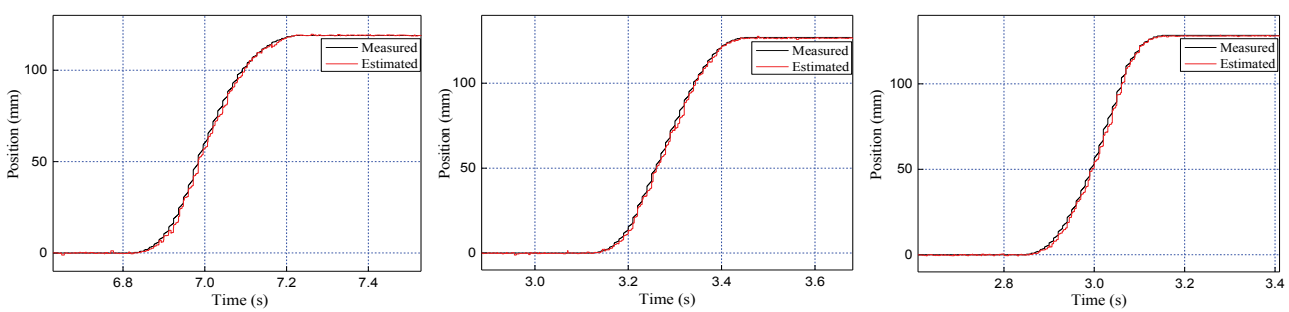

(a) (b) (c)

Fig. 15. Position estimation results of a DLSRM with different eccentricities (velocity: 0.45 m/s). (a) ε=0%. (b) ε=20%. (c) ε=40%.

TABLE II
ERRORS OF THE EXPERIMENTAL RESULTS

Eccentricity (%)	Velocity (m/s)	Maximum error (mm)	Average error (mm)	RMS error (mm)
0	0.15	1.47	-0.25	0.32
	0.30	2.63	-0.75	1.12
	0.45	5.34	-1.33	2.59
20	0.15	1.42	-0.26	0.43
	0.30	2.70	-0.81	1.22
	0.45	5.52	-1.47	2.86
40	0.15	1.55	-0.33	0.42
	0.30	2.75	-0.80	1.20
	0.45	5.75	-1.55	2.95

and estimated positions of the machine with an eccentricity of 0% and a mover velocity of about 0.15 m/s. Then the eccentricity of the prototype is adjusted to 20% and 40% and the corresponding prototype test results are given in Fig. 13(b) and Fig. 13(c).

In addition, the power supply voltage, turn-on position and turn-off position are kept unchanged and the motor load is reduced so that the velocity of the DLSRM reaches 0.30 m/s. Fig. 14 gives test results of the DLSRM prototype under different eccentricities. Fig. 15 shows results of the DLSRM in the case of a 0.45 m/s velocity. Table II shows errors of the measured results of the DLSRM sensorless control with different eccentricities under three kinds of velocities.

The following conclusions can be drawn from Table II.

(1) At the same velocity, a change of the eccentricity has little effect on the DLSRM position estimation. This means that the DLSRM position estimation method proposed in this paper is effective.

(2) With an increase of the mover velocity, the error of the DLSRM position estimation is increased. The main reason for this error is the same as the other position estimation methods based on VPIM, that is the effective number of injected pulses is decreased when the velocity becomes higher, and the neglect of the machine back-EMF.

VI. CONCLUSIONS

This paper proposes a novel sensorless control method for a DLSRM with different eccentricities. The key conclusions of this paper are as follows.

(1) A new position index, which is independent of machine eccentricities, is proposed for sensorless control systems through analyses of the magnetic circuit and finite element model. When compared with the position-eccentricity-inductance lookup-table, the new position index simplifies the computation and test process, and decreases the memory requirement of the controller chip.

(2) Based on the proposed position index, the starting and the low-velocity operation methods of DLSRMs with different eccentricities are designed. DLSRMs with different eccentricities (ε=0%, ε=20%, and ε=40%) are set to verify the proposed methods in the experiments. The test results show that changes of eccentricities have little influence on the proposed sensorless control of DLSRMs.

(3) The proposed sensorless control method is based on voltage pulse injection. The error increases with the mover velocity. Therefore, the proposed method is only suitable for DLSRMs at the starting and low-velocity operations. Sensorless control methods for a DLSRM with eccentricities at higher-velocities will be studied in the near future.

ACKNOWLEDGMENT

This research was supported by Natural Science Foundation of Jiangsu Province, China (Grant No. BK20170503), and Yangzhou city-Yangzhou University Joint Fund (SCX20170 20021).

REFERENCES

[1] J. Pan, Y. Zou, and G. Cao, "Investigation of a low-power, double-sided switched reluctance generator for wave energy conversion," *IET Renew. Power Gener.*, Vol. 7, No. 2, pp. 98-109, May 2013.

[2] D. Wang, X. Du, D. Zhang, and X. Wang, "Design, optimization, and prototyping of segmental-type linear switched-reluctance motor with a toroidally wound mover for vertical propulsion application," *IEEE Trans. Ind. Electron*., Vol. 65, No. 2, pp. 1865-1874, Feb. 2018.

[3] L, Qiu, Y. Shi, J. Pan, and G. Xu, "Networked H∞ controller design for a direct-drive linear motion control system," *IEEE Trans. Ind. Electron*., Vol. 63, No. 10, pp. 6281-6291, Oct. 2016.

[4] J. Amoros, P. Andrada, B. Blanque, and M. Marin-Genesca, "Influence of design parameters in the optimization of linear switched reluctance motor under thermal constraints," *IEEE Trans. Ind. Electron*., Vol. 65, No. 2, pp. 1875-1883, Feb. 2018.

[5] P. Acarnley, R. Hill, and C. Hooper, "Detection of rotor position in stepping and switched motors by monitoring of current waveforms," *IEEE Trans. Ind. Electron*., Vol. 32, No. 3, pp. 215-222, Aug. 1985.

[6] H. Yang, J. Kim, and R. Krishnan, "Low-cost position sensorless switched reluctance motor drive using a single-controllable switch converter," *J. Power Electron.*, Vol. 12, No. 1, pp. 75-82, Jan. 2012.

[7] S. Kuai, X. F. Li, X. H. Li, and J. Ma, "Variable coefficient inductance model-based four-quadrant sensorless control of SRM," *J. Power Electron.*, Vol. 14, No. 6, pp. 1243-1253, Nov. 2014.

[8] J. Cai and Z. Deng, "A position sensorless control of switched reluctance motors based on phase inductance slope," *J. Power Electron.*, Vol. 13, No. 2, pp. 264-274, Mar. 2013.

[9] H. Gao, F. Salmasi, and M. Ehsani, "Inductance model-based sensorless control of the switched reluctance motor drive at low speed," *IEEE Trans. Power Electron.*, Vol. 19, No. 6, pp. 1568-1573, Nov. 2004.

[10] I. H. AI-Bahadly, "Examination of a sensorless rotor-position-measurement method for switched reluctance drive," *IEEE Trans. Ind. Electron*., Vol. 55, No. 1, pp.

288-295, Jan. 2008.
[11] S. Zhao, N.C. Cheung, W. Gan, and J. Yang, "Position estimation and error analysis in linear switched reluctance motors," *IEEE Trans. Instrum. Meas.*, Vol. 58, No. 8, pp. 2815-2823, Aug. 2009.
[12] Q. Wang, H. Chen, T. Xu, J. Yuan, J. Wang, and S. Abbas, "Position estimation of linear switched reluctance machine with iron losses based on eddy-current effect," *IET Electric Power Appl.*, Vol. 10. No. 8, pp. 772-778, Sep. 2016.
[13] Q. Wang, H. Chen, T. Xu, R. Nie, J. Wang, and S. Abbas, "Influence of mover yoke and winding connections on unbalanced normal force for double-sided linear switched reluctance machine," *IET Electric Power Appl*., Vol. 10. No. 2, pp. 91-100, Feb. 2016.
[14] Q. Wang, H. Chen, T. Xu, Y. Yuan, J. Wang, and S. Abbas, "Inductance estimation method for linear switched reluctance machines considering iron losses," *IET Electric Power Appl*., Vol. 10. No. 3, pp. 181-188, Mar. 2016.
[15] Q. Wang, H. Chen, and R. Nie, "Unbalanced normal force reduction in the eccentric double-sided linear switched reluctance machine," *IET Electric Power Appl*., Vol. 10. No. 5, pp. 384-393, Jun. 2016.

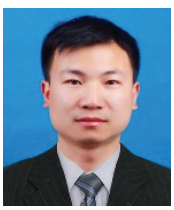

Qianlong Wang was born in Anhui, China, in 1988. He received his B.S. and Ph.D. degrees in Electrical Engineering from the China University of Mining and Technology, Xuzhou, China, in 2010 and 2016, respectively. He is presently working as a Lecturer at Yangzhou University, Yangzhou, China. His current research interests include the design and control of rotary and linear switched reluctance machines.

Zhengfei Wu was born in Jiangsu, China. He received his B.S. degree in Mechanical-Electronic Engineering from the Huaihai Institute of Technology, Lianyungang, China, in 2017, where he is presently working towards his M.S. degree. His current research interests include the design and control of switched reluctance motors.

Wei Jiang was born in Yangzhou, China, in 1980. He received his B.S. degree from Southwest Jiaotong University, Chengdu, China, in 2003; and his M.S. and Ph.D. degrees in Electrical Engineering from the University of Texas at Arlington, Arlington, TX, USA, in 2006 and 2009, respectively. From 2007 to 2008, he worked as a Senior Design Engineer at EF Technologies L.L.C. In 2010, he became a Lecturer at Yangzhou University, Yangzhou, China, where he founded the Smart Energy Laboratory and is presently working as an Associate Professor. His current research interests include digitalized power conditioning for renewable energy and energy storage devices, and the microscopic analysis of electromechanical energy conversion.